Title	Influence of pulsed laser deposition rate on the microstructure and thermoelectric properties of Ca3Co4O9 thin films
Author(s)	Sun, T.; Ma, Jan; Yan, Qingyu; Huang, Y. Z.; Wang, J. L.; Hng, Huey Hoon
Citation	Sun, T., Ma, J., Yan, Q., Huang, Y. Z., Wang, J. L. & Hng, H. H. (2009). Influence of pulsed laser deposition rate on the microstructure and thermoelectric properties of Ca3Co4O9 thin films. Journal of Crystal Growth, 311(16), 4123–4128.
Date	2009
URL	http://hdl.handle.net/10220/7518
Rights	

Influence of pulsed laser deposition rate on the microstructure and thermoelectric properties of $Ca_3Co_4O_9$ thin films

T. Sun, J. Ma, Q. Y. Yan, Y. Z. Huang, J. L. Wang and H. H. Hng*

School of Materials Science and Engineering, Nanyang Technological University, Singapore 639798

**corresponding author – Email: ashhhng@ntu.edu.sg; Tel: +65 67904140; Fax: +65 67909081*

Abstract

The effects of deposition rate on the microstructure and thermoelectric properties of $Ca_3Co_4O_9$ thin films fabricated by pulsed laser deposition (PLD) technique were investigated. X-ray diffraction (XRD) and high-resolution transmission electron microscopy (HRTEM) revealed that a fast deposition rate resulted in not only low crystallinity but also the existence of the Ca_xCoO_2 secondary phase. Formation of Ca_xCoO_2 was inevitable during the thin film growth, and this was discussed from both structural and compositional point of view. With longer deposition interval or with sufficient oxygen at a lower deposition rate, the Ca_xCoO_2 phase was able to transit into the desired $Ca_3Co_4O_9$ phase during the coalescence process. The quality of the thin films was further analyzed by electrical properties measurements. The $Ca_3Co_4O_9$ thin film fabricated at a

slower deposition rate was found to exhibit a low electrical resistivity of 9.4 mΩcm and high Seebeck coefficient of 240 μV/K at about 700ºC, indicating a good quality film.

Keywords:
A1. Surface Structure; A1. X-ray diffraction; A1. Atomic force microscopy; A3. Laser epitaxy; B1. Oxides

PACS Classification numbers:
61.05.cp X-ray diffraction
68.37.Ps Atomic force microscopy (AFM)
72.80.Ga Transition-metal compounds
73.50.Lw Thermoelectric effects

1. Introduction

Thermoelectric (TE) materials can directly convert heat energy into electricity power or vice versa. Therefore, they are of great interests for application in cooling and power generation devices [1]. The performance of a TE material is usually characterized by the dimensionless figure of merit ZT ($=S^2\sigma T/\kappa$, where S, σ, T and κ are the Seebeck coefficient, electrical conductivity, absolute temperature, and thermal conductivity, respectively).

Recently, misfit layered cobalt oxides have been identified to exhibit good thermoelectric properties and have received considerable attention thereafter due to their advantages over inter-metallic alloys in terms of high temperature stability and low toxicity [2, 3]. $Ca_3Co_4O_9$ (CCO) is among the best misfit layered cobalt oxides. Due to its good thermal stability at 1000K, intensive studies have been made to date. CCO crystal is composed of stacks of CdI_2-type CoO_2 layer alternating with rock-salt-type Ca_2CoO_3 layer along the c-axis and can be denoted as $[Ca_2CoO_3]^{RS}[CoO_2]_{1.62}$ [3]. The ZT value obtained for a single crystal reached ~0.83 at 1000 K [4]. However, it is very difficult to grow single crystals with large sizes. In addition, randomly

oriented ceramics show a relatively poor TE performance because CCO exhibits a high anisotropy in its TE properties.

Thin films, especially epitaxial ones, offer strongly oriented structure in contrast to bulk ceramics, and can exhibit intrinsic electrical properties similar to bulk single crystals. Moreover, thin film structure also benefits *ZT* improvement by increasing the thermopower due to quantum confinement effects and reducing the thermal conductivity due to lattice mismatches and scattering at surfaces and interfaces [5, 6]. CCO epitaxial thin films have been fabricated by RF sputtering and pulsed laser deposition (PLD) techniques on MgO (100), sapphire (0001) and Si (100) substrates [7-9]. However, thin films with high crystal quality have not been prepared and high temperature TE properties were also seldom reported. Moreover, an understanding on the CCO thin film growth mechanisms and the existence of secondary phase in the thin film structure [8, 9] are also limited. Although a number of PLD processing parameters have been investigated, the deposition rate, which is one of the most important parameters during thin film deposition process, has not received proper attention in earlier works on CCO thin film preparations. Here, we report our investigation of the deposition rate on CCO thin films, which indicated that a relatively low deposition rate is necessary to achieve a well-crystallized CCO structure as well as good thermoelectric properties. A faster deposition rate, on the other hand, results in the presence of the Ca_xCoO_2 secondary phase in the thin films. The growth mechanism of the CCO thin films will be discussed and explanation on the formation and further reaction of the secondary phase will also be presented from both the structural and chemical point of view.

2. Experimental Procedures

A $Ca_3Co_4O_9$ ceramic plate, synthesized by conventional solid state reaction, was used as the target for CCO thin films growth. Prior to the deposition, sapphire (0001) (*c*-plane) substrates were cleaned in ethanol and water followed by annealing at 1400ºC in oxygen gas flow to achieve an atomically-flat surface. The deposition was carried out by KrF excimer laser beam (Lambda Physik Compex, λ=248 nm) in 20 Pa oxygen pressure and the substrates were heated to 750ºC. The deposition rate could be related to many parameters such as laser energy density and target distance. In this work, the laser energy intensity was fixed at 1.2 J/cm^2 per pulse and the distance between substrate and target was 5 cm. The deposition rate was adjusted by varying the laser repetition frequency since this could be independently varied without giving rise to any side effects. The laser repetition frequency of 3, 4, 5 and 8 Hz were chosen, which correspond to deposition rates of ~2 to 5 nm/min.

The crystal quality, orientation, thickness and the surface morphology of the thin films were evaluated by X-ray diffraction (XRD), surface profiler, cross-sectional high-resolution transmission (HRTEM), and atomic force microscopy (AFM). The thin films thickness were about 100, 108, 80 and 110 nm for samples deposited using 3, 4, 5, and 8 Hz laser repetition respectively. XRD measurements were conducted using X'Pert PRO (PANalytical) with monochromatic Cu Kα radiation (λ=1.5406 Å) within 5-75º 2θ range. HRTEM observations were performed using a JEOL 2100F at 200 kV equipped with an Energy Dispersive X-ray (EDX) detector (Oxford Instruments, UK). For 3-Hz and 5-Hz-deposited thin films, TEM specimens were fabricated using a Focused Ion Beam dual beam system (Helios Nanolab 600 or Carl Zeiss

Nvision 40) and finally cleaned by using fine beam milling at 5 and 2 kV. Surface morphologies of CCO thin films were analyzed using a MFP-3D Stand Alone AFM (Asylum Research) at room temperature. The in-plane electrical resistivity (ρ) of the thin films was measured by dc four-probe method and the in-plane Seebeck coefficient (S) was measured by a conventional steady state method from room temperature to ~700ºC in helium atmosphere.

3. Results and discussion

Figure 1 shows the high-resolution XRD results of the CCO thin film deposited using 3 Hz laser repetition, and the inset shows the ω-scan rocking curve recorded around the (002) diffraction peak. The strong *c*-axis texture for the thin film revealed that the CCO thin film was hetero-epitaxially grown on the (0001) plane of α-Al_2O_3 substrate over the entire area of the film. From the seven {001} peaks of the film, the *c*-axis parameter was calculated to be 10.74(6) Å, which is in reasonable agreement with the bulk value (10.83 Å) [3] and other reported thin films (10.7 Å) [8-10]. The small full width at half maximum (FWHM) of the rocking curve (0.06º) is much smaller than reported value (0.83º) [11], which indicates that the films are well crystallized, i.e. of high crystallinity. Note that, by using the 3 Hz laser repetition, the deposition rate was only about 2 nm/min. This is a fairly low value as compared to normal PLD of other oxides which varies from 2 to15 nm/min [12, 13]. If the thin films were prepared at a higher deposition rate using higher laser repetition, the intensities of their XRD peaks decrease significantly as shown in Figure 2. In particular, for the thin films prepared using 5 Hz, peaks corresponding to the (001) and (003) planes are very weak while peaks corresponding to the (002) and (004) planes maintain high intensities with a slight shift to lower 2θ values. This XRD pattern is found to be similar to

that of the layer-structured Ca_xCoO_2 [14], which are made up of alternating Ca cation and CoO_2 layers.

Surface morphology of the as-prepared thin films was further analyzed using an AFM scanning a 5×5 μm square area (Figure 3). All three AFM images show tiny islands on the surface of the samples prepared using 3, 4 and 5 Hz laser repetition. It is obvious that for 3-Hz-deposited thin film, the island size is smaller and a smoother surface with a root mean square roughness (RMS) of ~4.2 nm was achieved. Meanwhile, by using faster deposition rates larger islands appeared on the sample surfaces, and a higher roughness (RMS: 6~8 nm) was obtained. These island-surface morphologies indicate that the thin film growth mechanism could be ascribed to either the Volmer-Weber growth mode (or island-growth mode) or the Stranski-Krastanov growth mode (S-K growth mode), which are common for hetero-epitaxial thin film growth [15]. For the S-K growth mode, the thin film growth mechanism starts with a layer-by-layer mode in the first stage, and this is followed by an island-growth mode after the critical thickness. The island formation on the surface of our thin films indicates a relatively high thermodynamic wetting energy of CCO film material on the sapphire substrate which could be ascribed to the large lattice mismatch (1.5% for CoO_2 layer/Al_2O_3 and 4.5% for the Ca_2CoO_3 layer/Al_2O_3) [11]. Since the nuclei growth or islands coalescence is a kinetic process in the latter stage of the thin film growth, a low deposition rate always caters for a good thin film quality with high crystallinity and smooth surface, while fast deposition rate results in high density of defects, random orientation of nuclei or even amorphous structure. It is obvious that our XRD and AFM results agree well with the above trends.

To further investigate the crystal structure of the thin films, especially the structure of the secondary phase, HRTEM analysis were performed with the incident beam parallel to the $[1\bar{1}00]$

of sapphire substrate on the cross-sectional area. Figure 4 (a) and (b) shows a well-ordered pile-up of layered structures in the 3-Hz-deposited CCO thin film. The *d*-spacing was evaluated to be 10.7 Å, which is consistent with the XRD analysis. The epitaxial relation of the film along the *c*-axis on the *c*-plane sapphire was found to be $[001]Ca_3Co_4O_9//[0001]Al_2O_3$. A transition region about 5 nm thick existed between the crystalline CCO thin film and the sapphire substrate. This region was found to consist of both secondary phase and amorphous structures. The secondary phase was adjacent to the surface of the substrate and was identified to be the Ca_xCoO_2 structure with a *c*-plane distance nearly half that of CCO. A small amount of stacking faults was also observed in the CCO structure. Nevertheless, the CCO structure still maintained good crystallinity on both sides of the stacking fault as shown in Figure 4 (c).

Figure 5 represents the HRTEM images of the 5-Hz-deposited thin film. Figure 5(b) shows another layered structure with 5.4 Å lattice *d*-spacing, which corresponds to the Ca_xCoO_2 phase [14]. The (001) plane of the Ca_xCoO_2 phase is still parallel to the (0001) plane of the sapphire substrate. However, such clear layered structure was only found in the region about 10 nm away from the film-substrate interface. Further away from the interface, a large amount of stacking faults were observed in the 5-Hz-deposited thin film, and the microstructure consists of a mixture of CCO, Ca_xCoO_2 and amorphous structure as shown in Figures 5(c) - (e). The images clearly show that the structure cannot maintain as either CCO or Ca_xCoO_2 on both sides of the stacking faults, but instead result in the formation of an amorphous phase (Figure 5c), curved layered lattice (Figure 5d) or even structures with other layered orientation (Figure 5e). All these correspond to a bad quality thin film. Ca_xCoO_2 or amorphous structure among CCO structures have also been reported in other CCO thin film fabricated by sputtering or PLD technique [8, 9]. However, no explanations were provided.

No layer-by-layer CCO growth region could be found at the first few atom layers near the substrate interface of the 3-Hz and 5-Hz deposited samples observed under HRTEM. Moreover, for the 3-Hz deposited films grown at a low deposition rate, CCO structures grew only after the transition layer, which was of mixed composition and a few atom layers thick. Herein, the CCO thin film growth could be further confirmed as an island-growth mechanism. The formation of the transition layer could be ascribed to the high wetting energy at the substrate-film interface and the high super-saturation during the PLD process. The stress from the lattice mismatch was totally released within the transition layer. The texture of CCO thin film was then achieved only by a self-assembling process without any epitaxial relationship from the substrate. Such observation was in good agreement with recent reports that highly textured CCO thin films were successfully fabricated on both Si (001) and glass substrate [9, 16]. Therefore, the quality of the CCO thin film is more related to the coalescence process where nuclei or islands unite while the atoms access to their thermodynamically stable sites.

From the structure point of view, similar to the structure of Na_xCoO_2 ($0.3 \leq x \leq 1$), the crystal structure of Ca_xCoO_2 is built up by alternating Ca cation and CoO_2 layers. Its structure is compared with the CCO structure in Figures 6(a) and (b). When the thin films stack up, it is easier to get a Ca_xCoO_2 structure since the *c*-axis lattice parameter of Ca_xCoO_2 is only about 5.4 Å [14], which is nearly half that of CCO (10.8Å). Meanwhile, the CoO_2 layer, composed of edge-shared CoO_6 octahedra, is a fundamental sub-unit in both CCO and Ca_xCoO_2 crystal structures. Due to the strong Co-O bonding, CoO_2 layer may be formed preferentially as compared to the Rock-salt layer. Thus, at stacking fault sites CoO_2 layers tend to extend further and a Ca_xCoO_2 structure is favored to release the local defect energy as illustrated in Figure 6(c). On the other hand, from the composition point of view, Ca_xCoO_2 may have a wide range of Ca:Co elemental

ratio, but contains lower O:Co ratio of 2:1 as compared to that of CCO which is 2.25:1. Thus, another possible reason for the Ca_xCoO_2 formation may lie in the lack of oxygen locally. Given enough time and sufficient oxygen supply, part of the CoO_2 layers are inclined to combine dissociative Ca and O atoms into the rock-salt layer of Ca_2CoO_3 and the Ca_xCoO_2 structure is able to transform into the CCO structure for lower thermodynamic energy as shown in Figure 6(d). The transition from Ca_xCoO_2 into CCO structure is a feasible process and has been reported elsewhere for the preparation of CCO [10, 17]. Nevertheless, a possible CCO thin film growth mechanism can be proposed as follows: During the coalescence process of nuclei, it is inevitable to have Ca_xCoO_2 structure at nuclei boundaries with high density of defects, or at some regions lacking in oxygen. Given enough ripening time, the defects can move to the surface of the thin film when top-layer nuclei unit together. The Ca_xCoO_2 can also combine with the ambient oxygen to transform into CCO structure. Both processes would result in a well aligned CCO thin film with *c*-axis texture. However, if the deposition rate is too high, too much mass will reach the surface within a unit time and the density of defects will be higher. Thus, more stacking faults will be embedded and accumulated at the boundaries, which will result in the generation of more Ca_xCoO_2 regions. Moreover, the opportunity to combine with ambient oxygen is quite small since the cations are buried under the new arriving layers and isolated from the ambient oxygen atmosphere. So, these embedded Ca_xCoO_2 structure are not able to transit into CCO and will remain within the thin film eventually. In addition, post annealing was also performed on the 5 and 8 Hz-deposited thin films at 800ºC in oxygen flow for 2 hours. This did not improve the CCO structure but instead increased the crystallinity of the Ca_xCoO_2 phase in the thin films. Thus, it is further confirmed that the embedded Ca_xCoO_2 structure can hardly transit into CCO and this

is consistent with reported fact that once formed, Ca_xCoO_2 is stable up to temperatures higher than 800ºC [17].

Finally, the electrical properties of the thin films deposited at 3, 4 and 5 Hz were compared and shown in Figure 7. Figure 7(a) shows the temperature dependence of the resistivity ρ for the thin films. Within the temperature range investigated, the 3-Hz-deposited thin film exhibits the lowest electrical resistivity, which ranges from 4.6 to 9.4 mΩcm, while the 4-Hz-deposited sample shows a slightly higher value. The room temperature resistivity of around 5 mΩcm obtained for these two thin films is fairly low among the values reported for both CCO thin films and single crystals [4, 10, 16], which indicates the good quality of these two thin films. Similar Seebeck coefficients *S* were also obtained for these two thin film samples. As shown in Figure 7(b), *S* value increased from 110 μV/K at room temperature to 240 μV/K at ~700ºC, which are comparable to reported data (110~240 μV/K) [4, 10, 16]. The slight difference in the electrical properties (ρ and *S*) between the two samples could be ascribed to the larger amount of stacking faults or lower crystallinity in the thin film prepared at a faster deposition rate. The thin film prepared by using 5 Hz repetition exhibited an electrical resistivity of 15~40 mΩcm and Seebeck coefficient of 120~180 μV/K Seebeck coefficient over the temperature range investigated. These properties correspond to a very bad quality thin film. According to its microstructure, the existence of the Ca_xCoO_2 structure could significantly affect the electrical properties of the thin film, since Ca_xCoO_2 exhibits a higher ρ and lower *S* as compared to CCO [18]. Also, defects and amorphous structures could lead to high scattering effects and reduction of carrier concentration, which both result in the higher resistivity obtained in the 5-Hz deposited thin films.

The presence of the structural defect was said to be helpful in enhancing the overall TE performance by reducing the thermal conductivity [16]. And it is indeed feasible to control the density of stacking faults in the CCO thin film by simply using different deposition rate. However, high density of stacking faults can also result in the formation of Ca_xCoO_2 phase with poor TE properties. Hence, additional study is still necessary to achieve the optimum amount of such stacking faults to obtain the best TE properties in CCO thin films using PLD.

4. Conclusion

In summary, high quality thin films of misfit layered cobalt oxide $Ca_3Co_4O_9$ were successfully fabricated by pulsed laser deposition with a deposition rate of ~2 nm/min using 3 Hz laser repetition. The XRD and HRTEM results revealed that a fast deposition rate leads to not only low crystallinity but also the formation Ca_xCoO_2 structures in the thin film. It was also concluded that the quality of the $Ca_3Co_4O_9$ thin film is strongly related to the coalescence process at the latter stage of the thin films growth. Slow deposition can restrain the formation of Ca_xCoO_2 secondary phase or help to convert the Ca_xCoO_2 into the CCO structure. $Ca_3Co_4O_9$ thin films fabricated by 3 and 4 Hz laser repetition showed electrical resistivity varying from 4.6 to 9.4 mΩcm and Seebeck coefficient varying from 110 to 240 μV/K over the investigated temperature ranging from room temperature to ~700ºC. These values were comparable to reported values and indicated that the films were of good quality.

Acknowledgments

The authors would like to thank Mr. Ke Chang and Mr. Lim Poh Chong for the high resolution XRD analysis. We are also grateful to Ms. Ong Lay Ting for TEM specimen preparations. This work was supported by the Agency of Science, Technology and Research (A*STAR) of Singapore.

References

[1] F. J. DiSalvo, Thermoelectric cooling and power generation, Science 285 (1999) 703-706.

[2] I. Terasaki, Y. Sasago, K. Uchinokura, Large thermoelectric power in $NaCo_2O_4$ single crystals, Phys. Rev. B 56 (1997) 12685-12687.

[3] A. C. Masset, C. Michel, A. Maignan, M. Hervieu, O. Toulemonde, F. Studer, B. Raveau, J. Hejtmanek, Misfit-layered cobaltite with an anisotropic giant magnetoresistance: $Ca_3Co_4O_9$, Phys. Rev. B 62 (2000) 166-175.

[4] M. Shikano, R. Funahashi, Electrical and thermal properties of single-crystalline $(Ca_2CoO_3)_{0.7}CoO_2$ with a $Ca_3Co_4O_9$ structure, Appl. Phys. Lett. 82 (2003) 1851-1853.

[5] L. D. Hicks, M. S. Dresselhaus, Effect of Quantum-Well Structures on the Thermoelectric Figure of Merit, Phys. Rev. B 47 (1993) 12727-12731.

[6] R. Venkatasubramanian, E. Siivola, T. Colpitts, B. O'Quinn, Thin-film thermoelectric devices with high room-temperature figures of merit, Nature 413 (2001) 597-602.

[7] T. Terada, Y. Yoshida, M. Ueno, Y. Takai, Preparation and properties of $[Ca_2CoO_3]_x[CoO_2]$ thin films using pulsed laser deposition, J. Ceram. Soc. Jpn. 110 (2002) 560-563.

[8] A. Sakai, T. Kanno, S. Yotsuhashi, A. Odagawa, H. Adachi, Control of epitaxial growth orientation and anisotropic thermoelectric properties of misfit-type $Ca_3Co_4O_9$ thin films, Jpn. J. Appl. Phys. 44 (2005) L966-L969.

[9] Y. F. Hu, W. D. Si, E. Sutter, Q. Li, In situ growth of c-axis-oriented $Ca_3Co_4O_9$ thin films on Si(100), Appl. Phys. Lett. 86 (2005) 082103.

[10] K. Sugiura, H. Ohta, K. Nomura, M. Hirano, H. Hosono, K. Koumoto, High electrical conductivity of layered cobalt oxide $Ca_3Co_4O_9$ epitaxial films grown by topotactic ion-exchange method, Appl. Phys. Lett. 89 (2006) 032111.

[11] H. W. Eng, W. Prellier, S. Hebert, D. Grebille, L. Mechin, B. Mercey, Influence of pulsed laser deposition growth conditions on the thermoelectric properties of $Ca_3Co_4O_9$ thin films, J. Appl. Phys. 97 (2005) 013706.

[12] Hanns Ulrich Habermeier, Thin films of perovskite-type complex oxides, Materials Today 10 (2007) 34-43.

[13] S. R. Gilbert, L. A. Wills, B. W. Wessels, J. L. Schindler, J. A. Thomas, C. R. Kannewurf, Electrical transport properties of epitaxial $BaTiO_3$ thin films, J. Appl. Phys. 80 (1996) 969-977.

[14] B. L. Cushing, J. B. Wiley, Topotactic routes to layered calcium cobalt oxides, J. Solid State Chem. 141 (1998) 385-391.

[15] J. S. Horwitz, J. A. Sprague, Film Nucleation and Film Growth in Pulsed Laser Deposition of Ceramics, in: D. B. Chrisey, G. K. Hubler (Eds), Pulsed Laser Deposition of Thin Films, Wiley-Interscience, New York, 1994, pp. 229-237.

[16] Y. F. Hu, E. Sutter, W. D. Si, Q. Li, Thermoelectric properties and microstructure of c-axis-oriented $Ca_3Co_4O_9$ thin films on glass substrates, Appl. Phys. Lett. 87 (2005) 171912.

[17] H. Itahara, W. S. Seo, S. Lee, H. Nozaki, T. Tani, K. Koumoto, The formation mechanism of a textured ceramic of thermoelectric $[Ca_2CoO_3]_{0.62}[CoO_2]$ on beta-$Co(OH)_2$ templates through in situ topotactic conversion, J. Am. Chem. Soc. 127 (2005) 6367-6373.

[18] T. Kanno, S. Yotsuhashi, H. Adachi, Anisotropic thermoelectric properties in layered cobaltite A_xCoO_2 (A=Sr and Ca) thin films, Appl. Phys. Lett. 85 (2004) 739-741.

Figure Captions

Figure 1. High-resolution XRD patterns of $Ca_3Co_4O_9$ thin film deposited by using 3 Hz laser repetition on *c*-plane sapphire substrate. The ω-scan rocking curve around the (002) diffraction peak is shown in the inset.

Figure 2. XRD patterns comparison of the thin films deposited using different laser repetition within a 5º~55º 2θ range using a high intensity XRD scanning.

Figure 3. Surface morphologies of the thin films prepared at (a) 3, (b) 4 and (c) 5 Hz laser repetition obtained using AFM scanning over a 5×5 μm area.

Figure 4. HR-TEM cross-section images of the $Ca_3Co_4O_9$ thin film deposited using 3 Hz laser repetition. The inset of (a) is the electron-diffraction pattern of a selected area with good crystallinity. Although stacking faults were observed in the thin film (c), the structures on both sides of the stacking faults still exhibit good crystallinity. *(Note: Pt is a protective layer deposited to prevent damaging the CCO thin film during the TEM specimen preparation process)*

Figure 5. HR-TEM cross-section images of the $Ca_3Co_4O_9$ thin film deposited using 5 Hz laser repetition. The inset of (b) is the fast Fourier transform image of a selected area of the secondary phase. Great amount of stacking faults resulted in (c) low crystallinity or amorphous structure, (d) layer curvature and (e) random orientation. *(Note: SiO_2 is a protective layer deposited to prevent damaging the CCO thin film during the TEM specimen preparation process)*

Figure 6. Crystal structures of (a) $Ca_3Co_4O_9$ and (b) Ca_xCoO_2, and the illustrations of (c) Ca_xCoO_2 formation instead of $Ca_3Co_4O_9$ to reduce the stacking fault energy, and (d) structure transition from Ca_xCoO_2 to $Ca_3Co_4O_9$ with combination of ambient oxygen during thin film growth.

Figure 7. Temperature dependence of electrical resistivity (a) and Seebeck coefficient (b) of the thin films deposited using 3, 4, and 5 Hz laser repetition.

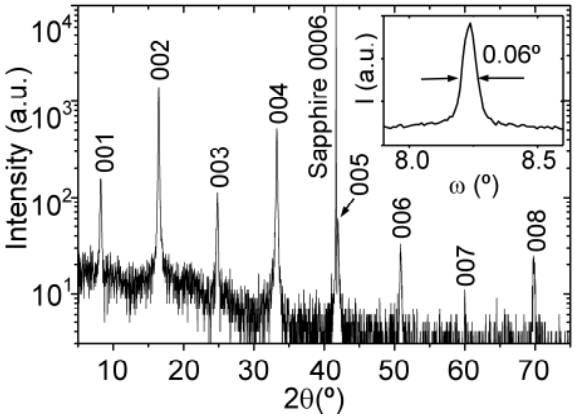
Intensity (a.u.)
10^4
10^3
10^2
10^1
001
002
003
004
Sapphire 0006
005
006
007
008
10
20
30
40
50
60
70
2θ(º)
I (a.u.)
0.06º
8.0
8.5
ω (º)

Figure 1

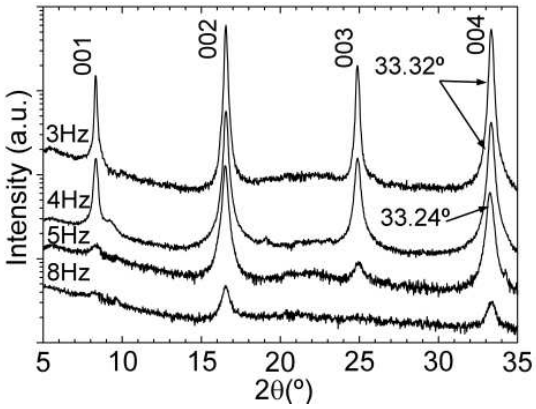
001
002
003
004
33.32º
33.24º
3Hz
4Hz
5Hz
8Hz
Intensity (a.u.)
5
10
15
20
25
30
35
2θ(º)

Figure 2

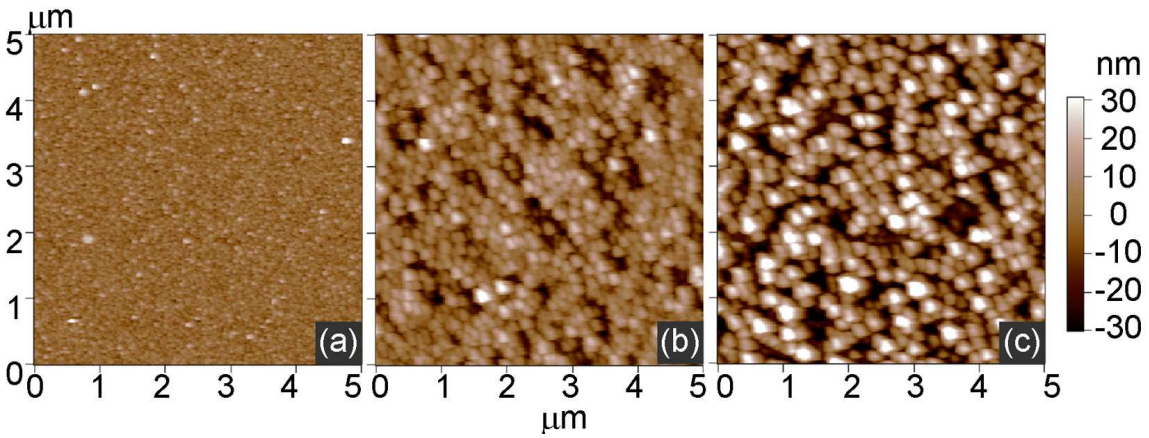

Figure 3

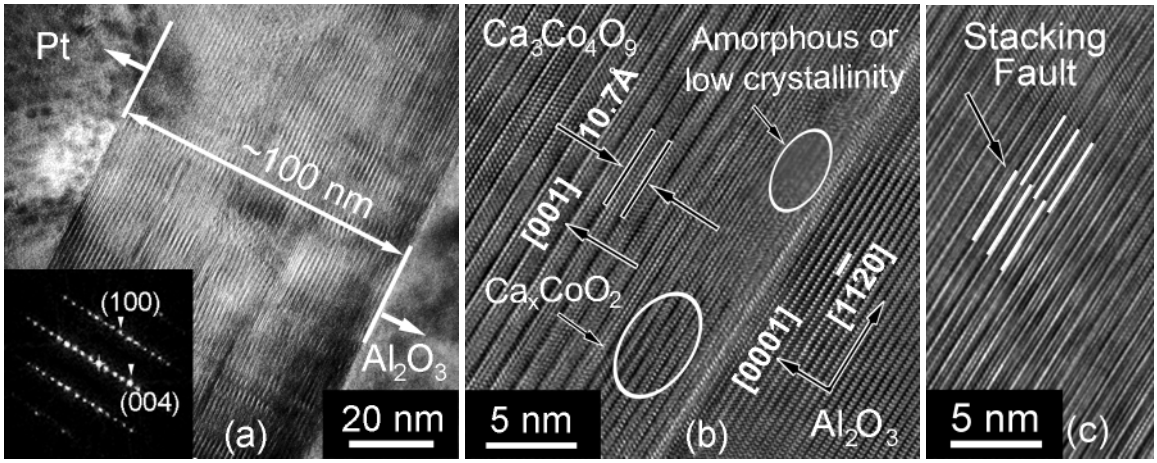
Pt
~100 nm
(100)
(004)
Al_2O_3
20 nm
(a)
$Ca_3Co_4O_9$
Amorphous or
low crystallinity
10.7Å
[001]
Ca_xCoO_2
[0001]
$[1\bar{1}20]$
5 nm
(b)
Al_2O_3
Stacking
Fault
5 nm
(c)

Figure 4

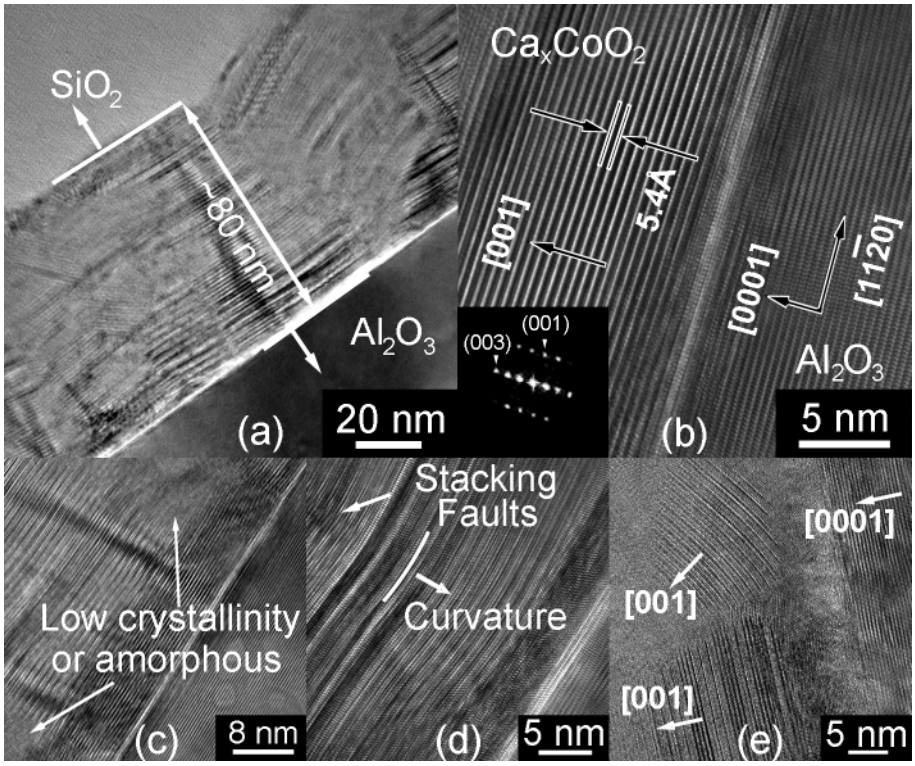
SiO2
~80 nm
Al2O3
(a)
20 nm
CaxCoO2
5.4A
[001]
(003)
(001)
[0001]
[1120]
Al2O3
(b)
5 nm
Low crystallinity
or amorphous
(c)
8 nm
Stacking
Faults
Curvature
(d)
5 nm
[0001]
[001]
[001]
(e)
5 nm

Figure 5

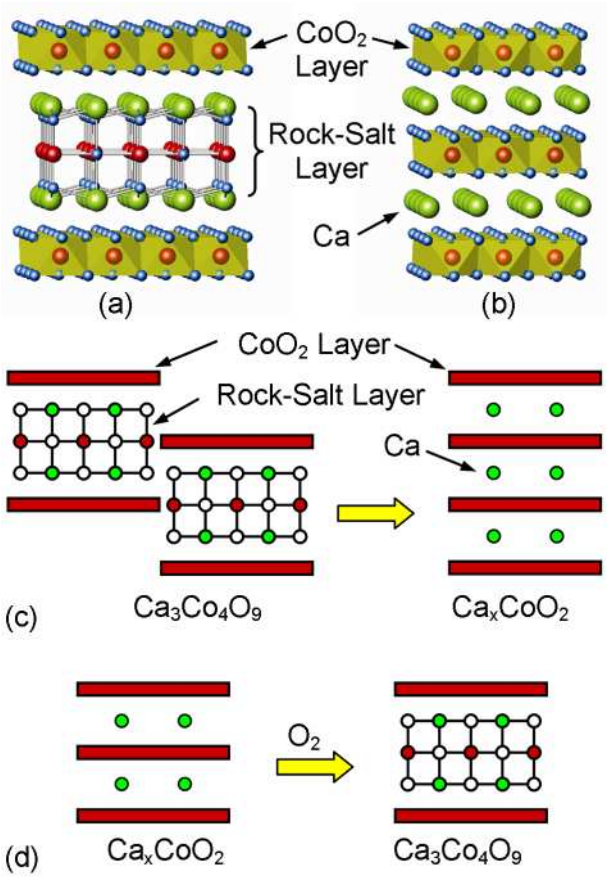
CoO2 Layer
Rock-Salt Layer
Ca
(a)
(b)
CoO2 Layer
Rock-Salt Layer
Ca
(c)
Ca3Co4O9
CaxCoO2
O2
(d)
CaxCoO2
Ca3Co4O9

Figure 6

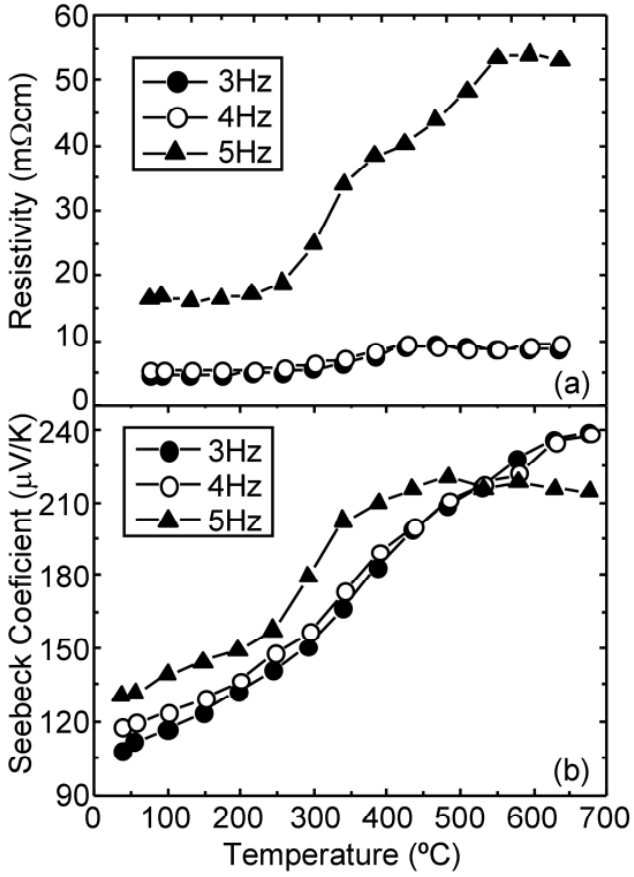
Resistivity (mΩcm)
3Hz
4Hz
5Hz
(a)
Seebeck Coeficient (μV/K)
3Hz
4Hz
5Hz
(b)
Temperature (ºC)

Figure 7